PAPER

Check for updates

Biomimetic multi-layer scaffolds with aligned polyurethane nanofibers and tailored hyaluronic acid/gelatin hydrogels for sustained methylprednisolone release in potential cardiovascular applications

Reyhaneh Farshbaf Shakib, [a] Masoumeh Haghbin Nazarpak, *[ab] Atefeh Solouk *[c] and Saeid Bahrami[b]

A key challenge in tissue engineering is designing three-dimensional (3D) biomimetic scaffolds that overcome the limitations of traditional 2D nanofibrous structures while promoting cellular activities and tissue regeneration. In this study, a multi-layered scaffold was developed by combining electrospun polyurethane (EPU) nanofibers containing methylprednisolone with hyaluronic acid (HA)–gelatin (G) hydrogels at varying ratios. The 3D structure enhanced porosity and mechanical properties. Increasing the HA : G ratio from 1 : 10 to 1 : 2 expanded pore size from ~208 μm to ~489 μm, creating a more favorable microenvironment for cell activities. Additionally, elongation at break increased from ~103% in EPU alone to ~196% in the EPU/HG (1 : 10), showing an improvement in the viscoelastic behavior of modified EPU. Controlled release of methylprednisolone was demonstrated over 80% delivery within 14 days. Biological evaluations with human umbilical vein endothelial cells (HUVECs) highlighted the scaffold's potential to support cell activities, including extensive filopodia anchoring. Also, cell viability assays confirmed the biocompatibility of all multi-layer scaffolds. These findings suggest that the developed biomimetic nanofiber/hydrogel scaffolds hold significant promise for cardiovascular tissue engineering applications.

1. Introduction

Cardiovascular diseases are the leading cause of death worldwide,[1,2] resulting in over 650 000 deaths each year in the United States alone.[3] They accounted for 27.4% and 43% of all deaths in 2019 in India and China, respectively.[4] In India, the cardiovascular mortality rate is 185 per 100 000 people, while in China it is 322 per 100 000 people. These statistics highlight the substantial burden of cardiovascular diseases across countries with large populations.[4] Due to the limited regenerative ability of cardiac tissue, surgical interventions such as organ transplantation and cell implantation may be necessary after heart attack.[1,3,5] However, due to challenges like donor shortages and the limited effectiveness of these methods in fully restoring heart function, tissue engineering approaches are often preferred.[2,6] Tissue engineering can potentially develop cardiovascular grafts or tissues that can be effectively implanted, addressing challenges related to the slow turnover rates of cardiovascular cell types.[1,2]

Scaffolds for cardiac tissue engineering should form a three-dimensional fibrous structure with anisotropic fiber orientation that can guide cell alignment and permit cell infiltration.[1,7,8] Biodegradable polymers stand out as highly attractive materials for cardiovascular tissue engineering applications with their adjustable degradation rates, optimal porosity, and elastomeric properties.[9] Scaffolds' design influences cell behavior and is vital for regeneration.[10,11] Electrospinning is a key technique for creating sub-micron to nanofiber scaffolds with high surface area.[12,13] Fibrous scaffolds mimicking the extracellular matrix (ECM) are crucial for tissue engineering, especially in tissues like tendons, vascular, cardiac, and muscles with aligned fibers.[11,14] Microstructure of the scaffold plays a fundamental role in directing cell behavior, and evidence indicates that the topography of electrospun nanofibers may guide cells differentiation toward specific phenotypes.[15,16] However, electrospun mats suffer from inherently limited cell infiltration due to their flat, 2D nature and small micro/nanoscale pores; which can be addressed by developing hybrid constructs that combine electrospun fibers with hydrogels.[17,18]

[a] New Technologies Research Center, Amirkabir University of Technology (Tehran Polytechnic), Tehran, Iran. E-mail: Haghbin@aut.ac.ir

[b] Department of Polymer and Color Engineering, Amirkabir University of Technology (Tehran Polytechnic), Tehran, Iran

[c] Department of Biomedical Engineering, Amirkabir University of Technology (Tehran Polytechnic), Tehran, Iran. E-mail: atefeh.solouk@aut.ac.ir

Polyurethane (PU) is a versatile polymer with a broad range of applications and properties due to its structure composed of soft and hard segments, making it a popular material in the biomedical field.[19] In particular, electrospun PU (EPU) nanofibers have shown great potential for cardiovascular tissue engineering due to their mechanical strength and elasticity; which closely mimic the native ECM for the endothelial cells and cardiomyocytes.[17] However, lack of appropriate biological properties can limit the PU scaffold–cell interactions including certain cell types such as endothelial and myocardial cells.[13] To overcome this limitation, researchers have explored modifications using natural macromolecules.[13] In this regard, the integration of PU with natural hydrogels is an effective strategy to enhance the biological functions of PU.

Natural hydrogels play a crucial role in tissue engineering due to their excellent plasticity and biocompatibility.[10,20] These highly water-swollen polymeric networks create a tissue-like environment that supports cell growth and allows for the diffusion of nutrients and waste.[10,21] Hyaluronic acid (HA), a glycosaminoglycan (GAG) structurally similar to the ECM, holds significant promise in tissue regeneration.[22,23] Natural materials like HA enable biomimicry, influencing the immunomodulatory response of host tissues through their peptide sequences, such as arginine-glycine-aspartic (RGD).[24] As a naturally derived polysaccharide, HA plays critical roles in biological processes, including angiogenesis and inflammation, leading to the development of various HA-based scaffolds to harness these properties.[25,26] It promotes cell proliferation and supports tissue-specific functions such as chondrogenesis, osteogenesis, neurogenesis, cardiogenesis, and angiogenesis. Additionally, HA modulates inflammation by binding monocytes and influencing the immune response, further enhancing its potential for regenerative medicine applications.[20,27]

On the other hand, gelatin (G), a natural polymer derived from collagen, offers several advantages for tissue engineering applications by enhancing the biocompatibility and biodegradability of fabricated scaffolds.[13] Its cost-effectiveness and lower antigenicity compared to biomolecules like collagen, along with the inclusion of RGD sequences resembling the native ECM, make gelatin a valuable macromolecule in tissue engineering.[13] While gelatin lacks sufficient mechanical strength and stability in aqueous media, it has found extensive use in cardiovascular tissue engineering due to its similarity to collagen, a prominent component of ECM in organs like vascular and heart.[9,28]

Despite hydrogels' advantageous properties, their mechanically weak nature presents a limitation, prompting efforts to enhance these properties through crosslinking.[10,29] Among the available crosslinking techniques, chemical methods are more effective than physical ones.[29] Carbodiimides, such as *N*-dimethylaminopropyl-*N'*-ethyl carbodiimide hydrochloride (EDC), are chemical crosslinkers that form amide bonds by activating carboxylic acids and reacting with free amines.[29,30] The combination of EDC with *N*-hydroxysuccinimide (NHS) is commonly used to improve the efficiency of crosslinking reactions.[31]

The fiber/hydrogel scaffolding approach not only enhances biocompatibility but also creates a 3D structure that augments bioactivity, contributing to improve overall performance.[32]

Additionally, these scaffolds containing EPU nanofibers have shown enhanced biomimetic scaffolds' mechanical properties, which may lead to a more favorable response toward tissue regeneration.[2] The exciting strategy of combining electrospun fibers and hydrogels creates biomimetic scaffolds that leverage the synergistic benefits of both structures and overcome their limitations;[29] offering enhanced structural support, improved cell behavior, and a more biocompatible microenvironment.

Moreover, controlling inflammation is critical in cardiac tissue engineering because the immune response after myocardial infarction orchestrates both the destructive and reparative phases of healing, and dysregulation of this tightly timed sequence leads to fibrosis, impaired remodeling, and heart failure and directly determining whether a scaffold will integrate successfully and support regeneration.[33–35] Inflammation after MI can be modulated using broad anti-inflammatory agents, targeted cytokine inhibitors, immunemodulatory biomaterials, pathways that regulate monocyte recruitment, strategies that promote the M1-to-M2 macrophage transition, ROS-responsive therapeutic systems, and emerging cell-based interventions.[33,35,36] Within this spectrum of approaches, glucocorticoids remain among the most widely used and mechanistically understood anti-inflammatory agents for cardiac repair. Among glucocorticoids, methylprednisolone (MP) stands out for its ability to suppress inflammatory mediators, reduce chemokine expression, clear apoptotic cells, and promote an anti-inflammatory macrophage phenotype.[33] In MI models, MP has shown therapeutic potential by reducing inflammation, minimizing injury, and enhancing blood flow and capillary formation.[33] For instance, Yao *et al.* developed a reactive oxygen species (ROS)-responsive PU loaded with MP, which showed antioxidant properties *in vitro* and significantly improved cardiac function and revascularization *in vivo*.[33]

In this study, fiber/hydrogel scaffolds were developed with a sandwich-like architecture, consisting of two hydrogel layers of HA and G surrounding a middle EPU mat containing the anti-inflammatory drug (*i.e.*, MP). This three-dimensional structure provides mechanical stability and topographical cues through the EPU fibers, while the hydrogel layers enhance cellular interaction. It is hypothesized that varying the HA : G ratio can modulate the scaffold's mechanical properties, swelling behavior, degradation rate, and drug release profile, ultimately yielding a biocompatible construct with improved endothelial cell adhesion and viability, with potential applications in cardiovascular therapies.

2. Materials and methods

2.1. Materials

MDI-polyester/polyether polyurethane (CAS No. 430218) was purchased from Sigma-Aldrich. Tetrahydrofuran (THF, Extra Pure Grade, CAS No. 109-99-9) and dimethylformamide (DMF, Extra Pure Grade, CAS No. 68-12-2) were obtained from Neutron (Iran). Hyaluronic acid (1.2×10^6 Da, purity 99.4%) was sourced from Chitotech (Iran), while gelatin (Type B, pure bovine, Bloom 160–180) was acquired from Faravari Darooi Gelatin Halal (Iran). 1-Ethyl-3-(3-dimethylaminopropyl) carbodiimide

hydrochloride (EDC-HCl, CAS No. 25952-53-8, purity >99%) and *N*-hydroxysuccinimide (NHS, CAS No. 6066-82-6, assay 98%) were purchased from Roth and Merck, respectively. Methylprednisolone (500 mg) was supplied by Ronak Pharmaceutical Company (Tehran, Iran). Glutaraldehyde (OHC(CH$_2$)$_3$CHO) and 3-(4,5-dimethyldiazol-2-yl)-2,5-diphenyl tetrazolium bromide (MTT) were obtained from Sigma-Aldrich.

Human umbilical vein endothelial cells (HUVECs) were obtained from Pasture National Cell Bank (Iran). Dulbecco's Modified Eagle's Medium (DMEM) was sourced from Gibco (Canada), and fetal bovine serum (FBS) was purchased from DNA Biotech Company (Iran). Trypsin-EDTA, penicillin–streptomycin, and isopropyl alcohol were acquired from Merck. Phosphate-buffered saline (PBS) was purchased from Medicago.

2.1.1. Nanofiber fabrication. Nanofibrous scaffolds were fabricated through the electrospinning technique, as previously described.[11] In summary, a solution consisting of 11% w/w PU dissolved in a blend of THF and DMF (50 : 50 v/v) was prepared at room temperature. The PU solution was loaded into a 5 mL plastic syringe fitted with a 22-G needle positioned at approximately 18 cm from the collector. The electrospinning process was performed under a high voltage of 18 kV with an injection rate of the solution at 0.8 mL h^{-1}. To fabricate electrospun mats containing MP drug, 40 mg mL^{-1} of MP was first added to the PU solution, as reported in a previous study.[36] The electrospun PU-drug (EPUD) nanofibers were produced under the same conditions as the pure EPU. Methylprednisolone was dissolved in the PU solution prior to electrospinning, resulting in encapsulation of the drug within the fiber matrix. To induce fiber alignment, a rotating collector was utilized at a speed of 2300 rpm, a parameter adapted and slightly modified from the study by Bahrami *et al.*[11] Additionally, random nanofibers were produced using a setting of 300 rpm. The drum diameter was 5 cm. The linear surface speed (*v*) was calculated as eqn (1):

$$\text{Linear surface speed (m s}^{-1}) = 2\pi r \times (\text{rpm}/60) \tag{1}$$

where *r* is the drum radius (m).

2.1.2. Hydrogel preparation. An aqueous solution of HA–G with a concentration of 5 w/v% was prepared by first dissolving G in distilled water using a 40 °C water bath for 20 min, followed by the addition of HA and stirring for 30 min. The blending ratios (w/w) of HA : G were set at 0 : 100, 1 : 10, 1 : 4, and 1 : 2, denoted G, HG (1 : 10), HG (1 : 4), and HG (1 : 2), as indicated in Table 1. Separately, solutions of EDC and NHS were prepared in

deionized water at room temperature with a 1 : 1 molar ratio. The molar ratio of EDC to the total amount of COOH groups in HA–G solution was set at 1 : 1, based on the crosslinking conditions reported by Bahrami *et al.*[29] Finally, 0.25 mL of each EDC and NHS solution was added to the HA–G mixture and gently stirred to initiate crosslinking.

2.1.3. Fiber/hydrogel scaffold assembly. The sandwich structural scaffold was prepared using a manual assembly; the bottom and top layers were hydrogel and the inner layer was nanofibrous EPU containing MP. This construct was obtained using multi-step process. In a silicone mold, a small amount of the HA–G solution containing EDC/NHS crosslinking agents, with previously mentioned ratios, was added as the base layer. Following this, the EPUD mat was carefully placed onto the hydrogel layer and immediately, the assembly was completed by covering the EPUD mat with an additional layer of hydrogel. Then, the scaffolds were stored at 4 °C for 24 h to achieve complete crosslinking of the hydrogels. Subsequently, the scaffolds underwent freezing at −20 °C and were subjected to a 24 h freeze-drying process. All the samples preparation conditions are summarized in Table 1. Also, the fabrication process of the multi-layered scaffold is shown in Fig. 1.

2.2. Characterization

2.2.1. Surface morphology. The morphology of the scaffolds was assessed using scanning electron microscopy (SEM; AIS-2100, Seron Technology). Before SEM imaging, scaffolds were sputter-coated with gold (SC7620, EMITECH) to enhance conductivity. Using ImageJ software (National Institutes of Health, USA), the average fiber diameter and fiber orientation were determined from SEM images. More than 100 randomly
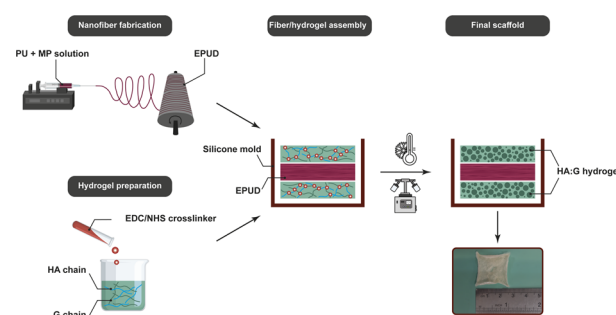

Fig. 1 Fabrication process of the multi-layered scaffolds.

Table 1 Sample codes and their preparation conditions

Sample code	PU concentration (w/w)	Drug concentration (mg mL^{-1})	HA–G concentration (w/v)	HA : G (w/w)	EDC/NHS molar ratio
EPU	11%	0	0%	0 : 0	0
EPUD	11%	40	0%	0 : 0	0
EPUD/G	11%	40	5%	0 : 100	1 : 1
EPUD/HG (1 : 10)	11%	40	5%	1 : 10	1 : 1
EPUD/HG (1 : 4)	11%	40	5%	1 : 4	1 : 1
EPUD/HG (1 : 2)	11%	40	5%	1 : 2	1 : 1

selected nanofibers were analyzed to calculate the fiber diameter and angle of fiber orientation, with the orientation determined by measuring the angle between the fiber and the horizontal line. Histograms were generated to illustrate the distribution of fiber orientation across the entire 0° to 180° range.

2.2.2. Porosity and pore size. The surface porosity of electrospun scaffolds was assessed using an image processing technique developed by Ghasemi-Mobarakeh *et al.*[37] In this approach, each grayscale SEM image of the fibers was converted into a binary image using ImageJ software with varying threshold values, and porosity was calculated across different layers. The surface porosity was then determined as the ratio of white pixels to the total number of pixels, which can be mathematically expressed as eqn (2):

$$\text{Porosity (\%)} = (1 - (n/N)) \times 100 \qquad (2)$$

where, n represents the number of white pixels and N is the total number of pixels in the binary image, respectively. To measure pore size, at least 30 pores from different SEM images were randomly selected, and an ellipse was fitted to each pore. The larger diameter of the ellipse was measured using ImageJ software to determine the pore size.[38]

2.2.3. Chemical composition. To assess the chemical composition of the scaffold surfaces, attenuated total reflectance Fourier transform spectroscopy (ATR-FTIR) analysis was conducted using the NICOLET iS10, Thermo Scientific. FTIR spectra were obtained in the wavenumber range of 4000 cm^{-1} to 550 cm^{-1} with a resolution of 4 cm^{-1}.

2.2.4. Water contact angle. In this test, water droplets with a volume of 5 μL were placed at three distinct points on the surface of each sample using a micro-syringe. After a duration ranging from 10–60 seconds, digital photographs were captured using a Sony digital camera. Subsequently, the contact angle between the water droplet and the surface was measured using Digimizer software.

2.2.5. Swelling ratio. The freeze-dried scaffolds underwent precise weighing (W_d) and were immersed in PBS at 37 °C for 24 h. Subsequently, excess surface fluid was delicately removed from the scaffolds using filter paper, and subsequent weighing (W_s) was conducted. The swelling ratio was determined using eqn (3):

$$\text{Swelling ratio (\%)} = ((W_s - W_d)/W_d) \times 100 \qquad (3)$$

2.2.6. Crosslinking density. The degree of hydrogel crosslinking was assessed by quantifying the free amine groups in the hydrogel using the 2,4,6-trinitrobenzene sulfonic acid (TNBS) colorimetric assay.[39] Briefly, 11 mg of dry samples were treated with 1 mL of 4 wt% NaHCO$_3$ (pH 8.5) and 1 mL of 0.5 wt% TNBS solution for 4 h at 40 °C. Following this, 3 mL of 6N HCl was added to each sample, and the mixture was incubated at 60 °C for 2 h to hydrolyze and dissolve any remaining sample residue. After cooling to room temperature, the hydrolysate was diluted with 5 mL of distilled water and extracted

with diethyl ether three times to remove unreacted TNBS. A 5 mL aliquot of the aqueous phase was then heated in a hot water bath for 15 minutes to evaporate any remaining ether. The aliquot was diluted with 15 mL of distilled water, and the UV absorbance was measured at 345 nm. All samples were compared to a blank, which was prepared by adding HCl before TNBS to prevent any reaction with the gelatin. The crosslinking density was calculated using eqn (4):

$$\text{Crosslinking density (\%)} = (1 - (A_{\text{crosslinked}}/A_{\text{non-crosslinked}})) \times 100 \qquad (4)$$

where, $A_{\text{crosslinked}}$ and $A_{\text{non-crosslinked}}$ represent the absorbance of non-crosslinked and crosslinked samples, respectively.

2.2.7. Weight loss. Weight loss kinetics of the scaffolds were assessed through immersion in PBS and subsequent incubation at 37 °C, with periodic PBS renewal every 2 days. At designated intervals (7, 14, 21, and 28 days), residual samples were extracted, subjected to washing to eliminate excess PBS, and subsequently freeze-dried. The weight loss percentage was quantified utilizing eqn (5):

$$\text{Weight loss (\%)} = ((W_i - W_t)/W_i) \times 100 \qquad (5)$$

Herein, W_i denotes the initial scaffold weight, while W_t represents the scaffold weight at each specific time point, respectively.

2.2.8. Drug release. The release of MP from scaffolds was investigated by cutting MP-loaded scaffolds into 1×1 cm^2 pieces and placing them inside an active dialysis bag with 5 mL of PBS. The bag was then immersed in a beaker containing 30 mL of PBS (pH 7.4) and maintained at 37 °C. Drug release was monitored at various time points up to 240 hours. At specific intervals, 1 mL of the PBS solution was withdrawn and replaced with fresh PBS. The collected solution was analyzed for released drug content using a UV spectrophotometer (Micro UV-vis Spectrophotometer, BOECO) at a wavelength of 246 nm. The concentration of released MP at each time point, determined from the standard curve of MP, was recorded. The percentage of cumulative MP release (E_r) was calculated using eqn (6):

$$E_r(\%) = \left(V_0 \times C_n + V_r \times \sum_1^{n-1} C_i \right) \bigg/ M_t \times 100 \qquad (6)$$

where, V_0 and V_r represent the volumes of the released and replaced media, respectively. M_t stands for the MP content encapsulated in the nanofiber scaffold, and C_n denotes the MP concentration in the sample.

2.2.9. Mechanical properties. The mechanical characteristics of the scaffolds were assessed through uniaxial tension testing conducted parallel to the fiber orientation using a SANTAM STM-1 machine. The testing involved applying tension at a displacement rate of 5 mm min^{-1} until failure. Three samples for each condition underwent analysis.

2.2.10. Biological evaluation. The biological activity of EPU, EPUD, EPUD/HG (1 : 10), EPUD/HG (1 : 4) and EPUD/HG (1 : 2) was investigated through cell morphology and viability using HUVECs on the scaffolds. In this study, high-glucose Dulbecco

Paper

modified Eagle medium (DMEM) with 10% FBS and 1% penicillin–streptomycin were used as a culture medium. Before cell seeding, scaffolds sterilized by immersion in 70% ethanol for one hour and then washed repeatedly with PBS to remove residual ethanol. Moreover, cells cultured on a tissue culture plate (TCP) were considered to be the control group.

2.2.10.1. Cell attachment and morphology. The HUVECs were seeded onto scaffolds at a density of 2×10^4 cells per well and incubated under standard conditions of 37 °C and 5% CO_2. After 24 hours, the cell-seeded scaffolds were rinsed with PBS and fixed using a 2.5% glutaraldehyde solution. To assess cell attachment and morphology *via* SEM, the fixed cells were dehydrated through a graded ethanol series (50%, 60%, 70%, 80%, 90%, and 100% v/v) and subsequently sputter-coated with gold.

2.2.10.2. Cell viability. The cytotoxicity of the EPU, EPUD, EPUD/HG (1 : 10), EPUD/HG (1 : 4), and EPUD/HG (1 : 2) scaffolds was assessed using the MTT colorimetric assay, which evaluates cell viability by measuring metabolic activity. This assay relies on the reduction of light yellow MTT to purple formazan, reflecting the cells' metabolic activity levels.[40]

HUVECs were seeded into a 96-well plate at a density of 10^4 cells per well in 100 μL of culture medium and incubated for 24 hours. After incubation, the medium was removed, and the wells were rinsed with PBS. MTT solution (0.5 mg mL^{-1} in PBS) was then added to each well and incubated at 37 °C for 4 h. Following this, the MTT solution was discarded, and the formazan crystals were dissolved in isopropyl alcohol. The optical density (OD) at 490 nm was measured using an ELISA microplate reader (Biotek-ELx808). Cell viability was calculated using eqn (7):

$$\text{Cell viability (\%)} = (1 - (\text{OD}_{\text{sample}}/\text{OD}_{\text{control}})) \times 100 \qquad (7)$$

2.2.11. Statistical evaluation. All experiments were performed at least three times and quantitative data were expressed as mean ± SD (standard deviation). The results were statistically compared with one-way ANOVA, using GraphPad Prism version 9 software (California, USA). A p-value <0.05 was set to be statistically significant. Statistically significant values were presented as $*p < 0.05$, $**p < 0.01$, $***p < 0.001$, and $****p < 0.0001$.

3. Results and discussion

3.1. Surface morphology

As observed in Fig. 2A, both EPU and EPUD fibrous samples exhibited uniform, smooth, and defect-free characteristics. The average fiber diameter of EPU and EPUD samples was 544 ± 171 nm and 498 ± 126 nm, respectively. Results showed that the addition of the drug to the polymer solution decreased the fiber diameter significantly, which can be attributed to drug-induced disruption of chain entanglement and decreased solution viscosity.[41] These factors increased free volume, leading to thinner jets during electrospinning and finer fibers.[41]

As shown in the fiber orientation graphs in Fig. 2, increasing the collector speed led to the production of fibers with a preferred orientation. For a drum diameter of 5 cm, the surface speeds were
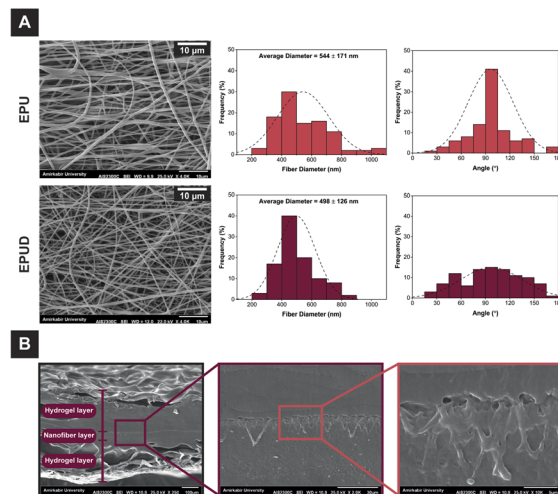

Fig. 2 (A) SEM images of EPU and EPUD and corresponding distribution of fiber diameter and orientation; (B) SEM cross-sectional image of the EPUD/HG (1 : 4) multi-layered scaffold.

approximately 6.02 m s^{-1} at 2300 rpm and 0.79 m s^{-1} at 300 rpm. These substantially different surface velocities promote fiber alignment at high speed and random deposition at low speed.[42] In the EPU sample, 63% of the fibers fell within the 80–120° range of alignment, while in the EPUD sample, 40% of the fibers were in this range, meaning that the distribution of fiber alignment in the EPU sample was more diverse compared to the EPUD sample.[38] The degree of fiber alignment is strongly governed by the relative velocities of the polymer jet and the collector surface. At low collector speed (300 rpm in our study), the linear surface speed of the drum is small relative to the jet's whipping motion; therefore, fibers are deposited in a chaotic manner and form a random network. Increasing the collector speed (2300 rpm) substantially increases the collector surface linear speed, which reduces the residence time of the jet on the collector surface, imposes a directional drag on the deposited fibers, and mechanically stretches and orients fibers along the rotational axis.[42,43] A study indicated that increasing the collector speed reduces the time required for the random alignment of charged fibers, resulting in enhanced fiber alignment.[38] Charged fibers, upon intersecting subsequent fibers, experience repulsive forces that lead to their random alignment. Therefore, an increase in the collector speed reduces the time for the random alignment of charged fibers and ultimately results in improved fiber alignment.[38] Drug incorporation decreased fiber diameter and alignment. Increased stretching forces elongated fibers and required a higher collector speed to prevent disorganization.[41] Also, viscosity and conductivity changes may further disrupt alignment.[41]

SEM cross-sectional image of the EPUD/HG (1 : 4) fiber/hydrogel sample is presented in Fig. 2. As observed, EPUD fibers were situated between two layers of HA–G hydrogel, resulting in uniform hydrogel width throughout the structure. The fibrous layer thickness was approximately 39 μm, while the overall scaffold thickness was 490 μm.

Fig. 3 depicts the distribution of pore size in hydrogel structures. The average pore size of the hydrogel scaffolds fell within

the range of 200–500 μm, which is favorable for cellular penetration.[44] The results from SEM images indicated that as the HA : G ratio increased, the size of the pores also increased from ∼208 μm to ∼489 μm. The pore size distribution graphs illustrated a significant increase in pore size with higher ratios of HA. The freezing process, known for utilizing ice as a porogenic template, was crucial in constructing a porous structure, in which water molecules played a significant role; the varying ratios of the HA : G influenced ice crystal growth during freezing.[45] Pure HA, abundant in hydroxyl groups, attracted water molecules more readily, leading to larger ice crystals during freezing than gelatin.[45] Consequently, increasing HA content promoted the formation of larger pore sizes in the resulting hybrid scaffolds.[45]

Porosity plays a critical role in tissue engineering scaffolds, significantly influencing cellular behavior, nutrient diffusion, and waste removal processes.[46] The surface porosity of samples EPU, EPUD, EPUD/G, EPUD/HG (1 : 10), EPUD/HG (1 : 4), and EPUD/HG (1 : 2) was 62.99% ± 9.39, 61,27% ± 9.57, 65.03% ± 6.67, 69.01% ± 3.85, 69.24% ± 2.30, and 71.89% ± 5.61, respectively. All samples exhibited porosity levels exceeding 60%, which is considered optimal for tissue engineering applications.[47] The results showed that addition of hydrogel layers slightly increased the porosity of the scaffolds. Furthermore, within the composite scaffolds, increasing the HA : G ratio resulted in a minor but noticeable rise in porosity. This effect was attributed to the formation of larger pores, a consequence of larger ice crystal formation during the freezing process. These larger pores created more void space within the structure, thereby enhancing overall porosity.[48]

3.2. Chemical composition

FTIR analysis was conducted to investigate the polyurethane's molecular interactions after adding MP and HA–G hydrogel

before and after crosslinking with EDC/NHS. The absorption spectra of cast PU and PUD solutions and hydrogels with different weight percentages of HA and G, before (named as nX-) and after crosslinking, in the wavelength range of 550–4000 cm^{-1} are shown in Fig. 4A. The characteristic peaks related to polyurethane were identified with N–H stretching at 3334 cm^{-1}, C–H stretching at 2943 cm^{-1}, and C=O stretching at 1700 cm^{-1}.[49,50]. The addition of MP slightly altered the carbonyl region, suggesting hydrogen bonding between PU and MP.[51] Also, the change in peak at 1661 cm^{-1} corresponded to the ketone groups of MP and confirmed its incorporation.[52] These shifts indicated that the drug was successfully integrated into the polyurethane matrix, primarily through hydrogen bonding, without significantly disrupting the polymer structure.

The broad absorption band around ∼3300 cm^{-1}, corresponding to hydrogen-bonded N–H stretching, was used as the normalization reference for FTIR spectra because it is minimally affected by the extent of crosslinking.[53] For the HA–G hydrogels, amide I (∼1631 cm^{-1}), amide II (∼1529 cm^{-1}), and amide III (∼1240 cm^{-1}) bands were observed, corresponding to C=O stretching and N–H bending vibrations, which reflect the secondary structure and triple-helical organization of gelatin.[29] Following normalization, the crosslinked hydrogels exhibited higher Amide I and Amide II peak intensities compared to the uncrosslinked samples (Fig. 4B). This increase reflects the formation of additional amide bonds during the carbodiimide-
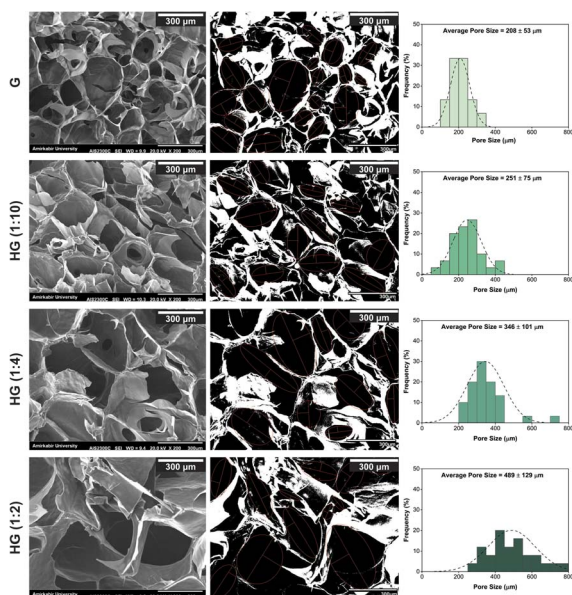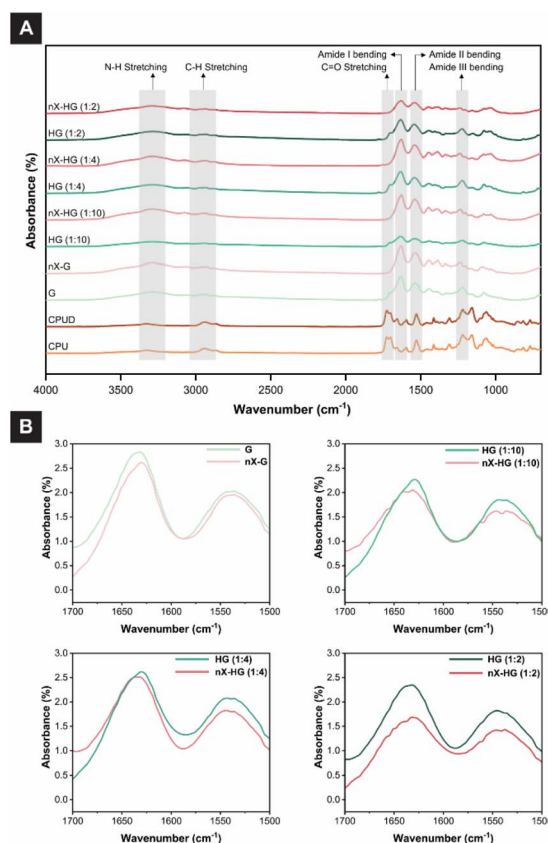

Fig. 3 SEM and binary representation for porosity and pore size measurement of HA–G hydrogels with different HA : G ratio and pore size distribution graphs.

Fig. 4 (A) FTIR spectra of HA–G hydrogels with different HA : G ratios, non-crosslinked and crosslinked with EDC/NHS. (B) Amide I and II peaks in HA–G hydrogels.
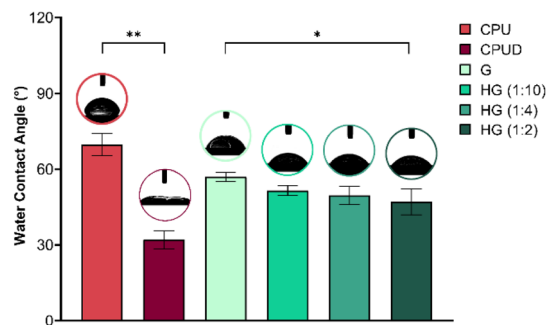
Fig. 5 The contact angle of PU, PUD, and HA–G hydrogel film with different HA : G ratios. $*p < 0.05$, $**p < 0.01$ and $n = 3$.

mediated crosslinking reaction, which enhances the overall amide-related absorbance.[53] The spectrum also exhibited a peak at 2943 cm^{-1}, corresponding to N–H stretching vibrations with C–H bonds.[29] Also, peaks at 1455 cm^{-1} and 1080 cm^{-1} were associated with ester linkages (C–O stretching and –CH bending). Symmetric and asymmetric carboxylate stretches were observed at 1414 cm^{-1} and 1614 cm^{-1}.[45] Overall, these results along with the TNBS assay confirm the successful formation of the crosslinked network and presence of both HA and gelatin in the hydrogel, supporting the intended structural integrity of the scaffold.

3.3. Water contact angle

Since surface hydrophilicity significantly influences biological interactions such as adhesion, proliferation, and migration of cells, the contact angle of water droplets on the sample surface was measured to assess surface hydrophilicity.[54] The addition of MP and hydrogel samples with different HA : G ratios was expected to change the surface properties of the samples. As shown in Fig. 5, the contact angle of PU film was less than 70°, similar to the results reported by Eivazi Zadeh *et al.*[55] A significant decrease in the contact angle was observed with the addition of the MP to the PU, which can be attributed to the presence of the hydrophilic groups of the MP in the PUD film, enhancing its wettability.[52] In all hydrogel samples, a contact angle of less than 70° was observed, indicating a hydrophilic nature of the HA–G structure. Moreover, a significant decrease in the contact angle was noted with the increase in HA : G ratio.
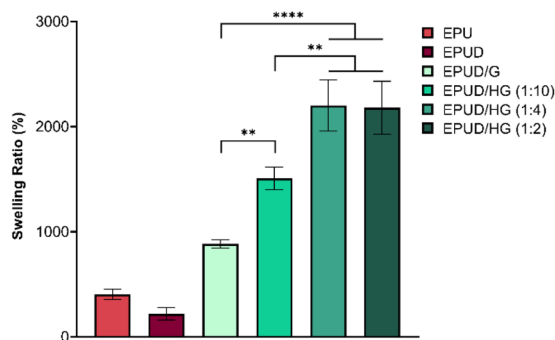

Fig. 6 Swelling ratio of multi-layered scaffolds with different HA : G ratios after 24 h. $**p < 0.01$, $****p < 0.0001$ and $n = 3$.

This finding was due to the increased hydrophilic groups in the HA–G structure.[52] Samples with a higher HA : G ratio had the lowest contact angle, indicating greater hydrophilicity of hyaluronic acid compared to gelatin.[56]

3.4. Swelling ratio

The water absorption capability is a fundamental characteristic of tissue engineering scaffolds that can indirectly reflect their mass transfer properties.[57] The swelling ratio of the samples after 24 hours is depicted in Fig. 6. With an increase in the HA : G ratio from 1 : 10 to 1 : 2, the swelling ratio of the scaffold increased from 900% to 2246%. This was attributed to the increased hydroxyl groups in the fiber/hydrogel structure and the enlargement of pore size in the scaffold.[57] Hyaluronic acid, due to its numerous hydrophilic groups (*e.g.*, –COOH and –OH), which carry a negative charge, exhibited a high water absorption capacity. Over time, water permeability within the polymer network improved, leading to greater swelling. The high hydrophilicity of the scaffold improved the interaction between cells and the scaffold.[52,57,58] Despite high swelling ratios, no structural damage, fragmentation, or delamination was observed during the swelling process. The HA–G network remained cohesive, and the presence of the aligned PU fiber layer reinforced the construct, allowing it to maintain its shape and mechanical integrity during handling. The scaffolds could be manipulated with tweezers without tearing, indicating that the swelling primarily reflects the hydrophilic nature of HA rather than structural instability.

Water absorption capacity of hydrogels is primarily influenced by the hydrophilic group content, the pore size of the structure, and their crosslinking density.[57] The absorbed water by the hydrogel increases the volume of the scaffold. The crosslinking bonds restrict the expansion of the hydrogel. Consequently, a higher density of lateral bonds leads to less water absorption.[29] It is worth mentioning that according to equilibrium swelling theories of mutually interacting polymer networks, such as the Flory–Rehner model, two opposing forces determine the swelling behavior of hydrogel structures. Firstly, thermodynamically compatible polymer chain and swelling-promoting liquid forces; and secondly, the restoring force of the polymer chains. The balance between these opposing forces leads to a swelling equilibrium.[59]

3.5. Crosslinking density

Crosslinking of gelatin-based hydrogels with EDC/NHS involves reactions between amine and carboxylic groups in gelatin, forming amide bonds.[48] In HA–G hydrogels, this reaction might occur between carboxylic groups of hyaluronic acid and amine groups of gelatin.[60] EDC activates carboxylic groups in hyaluronic acid into *O*-acylisourea intermediates, leading to amide linkages through nucleophilic attacks by amine groups in gelatin (Fig. 7A).[61,62] NHS stabilizes these reactions, preventing rearrangement and ensuring effective crosslinking.[24,63] Also, Fig. 7B shows that the HA–G hydrogel layer adhered to the polyurethane surface primarily through hydrogen bonding. These interactions occur between the urethane groups of PU and the hydroxyl, and amide groups present in HA and gelatin.[64]
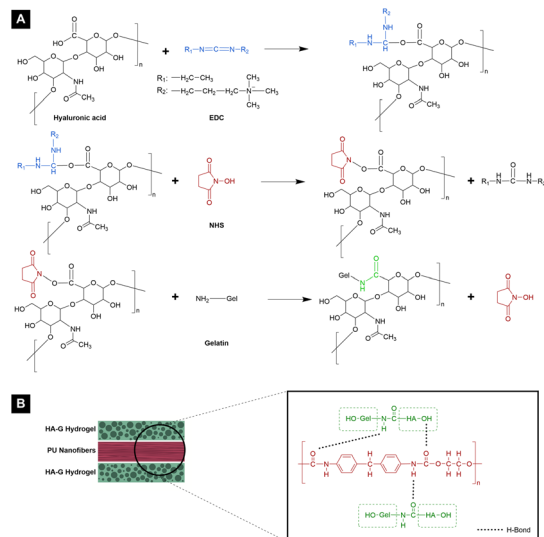
Fig. 7 (A) Schematic of the crosslinking reaction between hyaluronic acid and gelatin using EDC/NHS, (B) intermolecular interactions between PU and HA–G hydrogel.

Fig. 8 Crosslinking density of HG hydrogels with different HA : G ratios crosslinked with EDC/NHS. $**p < 0.01$, $***p < 0.001$ and $n = 3$.

As Fig. 8 shows, the crosslinking density displayed an overall decreasing trend with the increasing HA : G ratio. These findings were consistent with the results shown by Zhang *et al.* and Choi *et al.*.[45,62] It has been reported that scaffolds with higher content of HA possess lower crosslinking efficiency.[45] HA, as a non-sulfated glycosaminoglycan, has only two functional groups, hydroxyl and carboxyl, making it less reactive with crosslinking agents like EDC. In certain cases, chemical modifications are necessary to activate these groups for more effective cross-linking.[45] Moreover, the observed decrease in crosslinking degree with increasing HA content is likely due to EDC competitively activating carboxyl groups of both gelatin and HA simultaneously, thereby reducing overall crosslinking efficiency.[62]

3.6. Weight loss

The weight loss profile of tissue engineering scaffolds is a critical characteristic that influences their performance. Since scaffolds mimic the natural ECM of tissue, their weight loss rate must align with the rate of new tissue formation. To support cell behavior and tissue regeneration, scaffolds should maintain sufficient structural integrity throughout the healing process.[13,65] The rate of weight loss for all scaffolds was investigated in PBS solution at 37 °C for a period of four weeks.

Fig. 9 illustrates the degradation profile of EPUD and all composite scaffolds in PBS. As can be seen, EPUD exhibited a weight loss of approximately $7.3 \pm 2.3\%$ over the four weeks. In contrast, the weight loss percentage of all composite scaffolds exceeded 83%. This marked a significant difference in weight loss between EPUD and the composite scaffolds. It was also shown that in the first week, there was a significant difference between EPUD/HG (1 : 2) and both EPUD/G and EPUD/HG (1 : 10). However, in the subsequent weeks, mass loss percentage continued to increase without significant differences among samples with varying HA : G ratios. There was a clear trend between weight loss percentage and HA : G ratio;
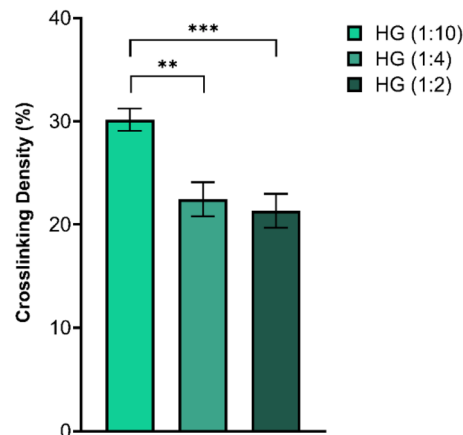
the higher ratios of HA : G, the weight loss percentage increased.

Cardiovascular regeneration can take up to 1–3 months, with the early 2–6-week period being critical for scaffold support and cellular activity. A 4–6 week degradation window has previously been reported as appropriate for hydrogels used in myocardial tissue engineering.[13,66] Therefore, the observed degradation profile supports early regenerative processes while the PU fiber layer maintains structural integrity during subsequent remodeling.

Hydrogel degradation depends on several factors, including hydrogel composition, crosslinking density, and environmental factors.[67] According to Zhang *et al.*, an increase in hyaluronic acid content within composite scaffolds correlates with a higher weight loss rate.[45] Additionally, the weight loss behavior of hydrogels is closely linked to their water uptake capacity.[68] As demonstrated in the swelling ratio section, hyaluronic acid is more hydrophilic than gelatin; thus, increasing the HA : G ratio (*i.e.*, the amount of HA relative to G) leads to higher fluid uptake by the scaffold, resulting in a higher weight loss percentage.[68] Moreover, crosslinking density decreases as the HA : G ratio increases, *a* factor that also influences weight loss. It has been reported that higher crosslinking density leads to lower weight loss in hydrogels.[67,69]

While weight-loss behavior at 37 °C reflects the scaffold's stability under physiologically relevant conditions, thermal
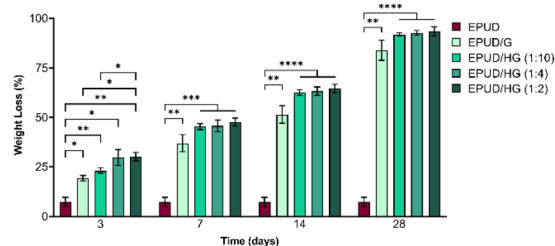

Fig. 9 Weight loss percentages of multi-layered scaffolds with different HA : G ratios during 28 days. $*p < 0.05$, $**p < 0.01$, $***p < 0.001$, $****p < 0.0001$, and $n = 3$.
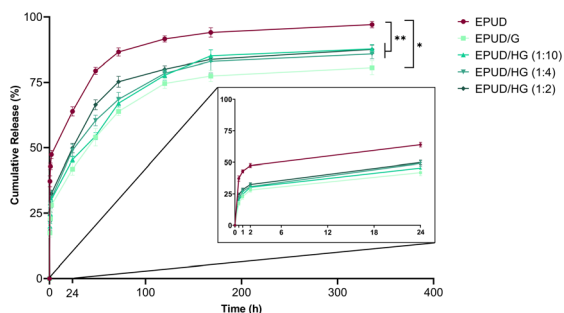
Fig. 10 Cumulative release profile of multi-layered scaffolds with different HA : G ratio during 14 days. $*p < 0.05$, $**p < 0.01$, and $n = 3$.

analyses such as TGA and DSC were beyond the scope of the current study. We acknowledge this limitation and these analyses will be considered in subsequent studies to further elucidate the scaffold's thermal and structural stability.

3.7. Drug release

Fig. 10 presents the cumulative drug release profiles of various samples as a function of time. The initial drug release behavior exhibited an initial burst release phase within the first few hours, followed by a gradual decline in the release rate. After two weeks, the cumulative percentage of released methylprednisolone in the samples EPUD, EPUD/G, EPUD/HG (1 : 10), EPUD/HG (1 : 4), EPUD/HG (1 : 2), was $97.1 \pm 1.3\%$, $80.6 \pm 2.7\%$, $87.8 \pm 1.7\%$, $85.9 \pm 1.9\%$, and $87.6 \pm 1.6\%$, respectively.

The burst release observed during the first two hours was attributed to the rapid influx of PBS into the scaffold's pores, which accelerated initial drug release. Once diffusion equilibrium was reached, the release rate continued at a slower pace.[52]

Among all samples, EPUD exhibited the highest cumulative drug release in PBS after two weeks, with statistically significant differences compared to other samples. The incorporation of a hydrogel layer reduced the final drug release, as it acted as a physical barrier through which the drug had to diffuse.[52] Although no significant difference was observed in the cumulative release among the multi-layer scaffolds, a higher HA : G ratio tended to accelerate the release rate. This trend corresponded directly with the findings from the weight-loss studies, which demonstrated that scaffolds with higher HA content underwent greater mass loss over time. As described in the degradation analysis, hyaluronic acid's higher hydrophilicity promotes greater water uptake, leading to increased swelling, faster hydrogel erosion, and consequently higher weight

loss.[45,68] The accelerated degradation observed in high-HA formulations reduces crosslinking density and weakens the hydrogel network, thereby facilitating faster diffusion pathways for the drug.[67,69] Thus, the increased cumulative drug release in scaffolds with higher HA : G ratios can be attributed to enhanced fluid uptake, increased hydrogel degradation, and lower crosslinking density, the same mechanisms driving their faster weight loss. Together, these factors contribute to the observed increase in drug release rate with increasing HA : G ratios.

Drug release kinetics were further analyzed using first-order, Higuchi, and Korsmeyer–Peppas (K–P) models to better understand the underlying release mechanism (Table 2). Kinetic analysis showed that the Korsmeyer–Peppas model provided the best fit for all samples, with R^2 values between 0.983 and 0.990, significantly higher than those obtained from first-order or Higuchi models. The release exponent n ranged from 0.154 to 0.237, indicating a predominantly Fickian diffusion mechanism for methylprednisolone release. Incorporation of hydrogel layers slightly increased the n value compared to EPUD alone, suggesting that polymer swelling and relaxation contributed modestly to drug transport; however, diffusion remained the dominant mechanism ($n < 0.45$). These findings support that the composite hydrogels alleviate burst release and provide a more regulated diffusion-controlled profile, consistent with the observed cumulative release trends.[70,71]

While the *in vitro* release profiles provide insight into the scaffold's controlled-release capabilities, true bioavailability can only be determined through *in vivo* pharmacokinetic evaluation, which was beyond the scope of the present study. Nevertheless, the controlled release observed suggests potential for enhanced local drug availability in a therapeutic setting, warranting further investigation in future *in vivo* studies.

3.8. Mechanical properties

Mechanical properties of scaffolds play a vital role in creating engineered scaffolds.[38] The properties of the membranes are particularly important as they provide temporary scaffolds for cellular behavior, such as ECM secretion, cell spreading, and cell adhesion.[72,73] Since myocardial tissue is subjected to mechanical tension, the mechanical properties of the scaffolds should be strong enough to withstand physiological conditions.[50,74] The maximum tensile strength to failure, elongation at break, and Young's modulus of scaffolds were reported in Fig. 11.

As shown in Fig. 11A and B, the incorporation of hydrogel layers resulted in a significant reduction in mechanical

Table 2 Fitting results of the MP release data to different kinetic equations

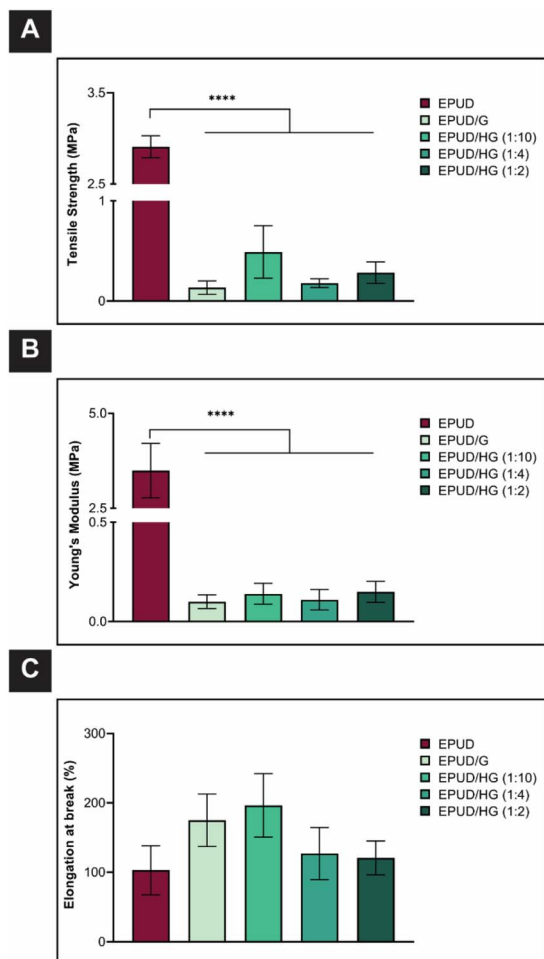| Sample	First-order		Higuchi		Korsmeyer–Peppas		
	k (h^{-1})	R^2	k_H (h$^{-1/2}$)	R^2	k (h^{-n})	n	R^2
EPUD	0.0035	0.7312	7.434	−0.6395	0.4221	0.1544	0.9850
EPUD/G	0.0041	0.8178	5.826	0.5388	0.2201	0.2375	0.9834
EPUD/HG (1 : 10)	0.0050	0.8713	6.240	0.5635	0.2416	0.2305	0.9854
EPUD/HG (1 : 4)	0.0043	0.8136	6.266	0.4053	0.2592	0.2194	0.9908
EPUD/HG (1 : 2)	0.0043	0.7777	6.484	0.2850	0.2818	0.2098	0.9863

Fig. 11 Tensile and elongation properties of EPUD and fiber/hydrogel multi-layer scaffolds: (A) tensile strength; (B) Young's modulus; and (C) elongation at break. ****$p < 0.0001$, and $n = 3$.

properties. Specifically, the maximum tensile strength decreased from 2.9 MPa in EPUD to 0.1 MPa in EPUD/G, while the Young's modulus dropped from 3.5 MPa in EPUD to 0.1 MPa in EPUD/G. Human myocardium has a tensile strength of 3–15 kPa and an end-diastolic Young's modulus of 0.2–0.5 MPa. The EPUD exhibited higher tensile strength and Young's modulus than native tissue; however, incorporation of hydrogel layers reduced these values, consistent with previous reports.[75] Among other samples, EPUD/HG (1 : 2) has the nearest Young's modulus to the native human myocardium (0.15 MPa). Although the tensile strength of the scaffolds is higher than that of native myocardium, this ensures sufficient structural support for cell seeding and manipulation.[13,75]

Generally, hydrogels exhibit weaker mechanical properties compared to electrospun fibers. The size of pores plays an essential role in defining the mechanical qualities of a material. Pores are generally considered imperfections, and when hydrogel layers are added, the size of the pores and overall porosity increase. As a result, the density of the scaffold decreases, and there is less polymer to withstand mechanical tension.[22,50] However, there was no significant difference in the tensile strength and Young's modulus of scaffolds with

different HA : G ratios. As shown in Fig. 11C, the addition of hydrogel layers increased the elongation at break from 103% in EPUD to 175% in EPUD/G, indicating enhanced flexibility, which is important for accommodating cyclic mechanical strain in cardiac tissue.[75] This improvement also contributed to an increase in the viscoelastic behavior of the fibers. The hydrogel penetrated the fiber network, acting as an adhesive that promoted cohesion among fibers and facilitated effective load transfer between scaffold components.[54] Together, these results suggest that the scaffolds provide a mechanically compatible environment for myocardial cells while maintaining sufficient structural support. When designing biomaterials for specific applications, electrospun fibers and hydrogels can work together to create a beneficial interplay. By using various manipulation methods, these controllable variables can be tailored to engineer the mechanical and physical properties of the material. Incorporating hydrogels has the potential to enhance the durability of electrospun fibers. Similarly, adding a fiber component can improve the mechanical properties of hydrogels while maintaining their beneficial features.[32,54]

3.9. Biological evaluation

3.9.1. Cell morphology. Biomaterials and scaffolds interact with cells, and their success depends on how well cells adhere to the surface of the biomaterials, which influences cell behavior.[55] A cytocompatible tissue engineering scaffold facilitates important cellular activities such as attachment, proliferation, ECM secretion, and differentiation.[76] To assess the behavior of cells on the scaffolds, HUVECs were cultured on the samples for 7 days, and their morphology was examined using SEM.

Polyurethane, a widely recognized biocompatible synthetic polymer, has been extensively used to create cardiovascular scaffolds.[5,55] SEM images of EPU and EPUD scaffolds showed that HUVECs adhered well to their surfaces (Fig. 12A). Previous studies have suggested that biocompatible nanofibrous substrates support cell attachment by replicating the fibrillar structure of the ECM.[17] The high aspect ratio of the electrospun mats, with their closer resemblance to the ECM structure, resulted in cells adopting a broad morphology with more filopodia, facilitating better cell-matrix interactions.[55] As noted earlier, aligned nanofibers can influence cell morphology, guiding cells to elongate along the direction of fiber alignment.[11] Given that EPU fibers exhibited slightly higher alignment compared to EPUD, HUVECs displayed more elongation in the direction of the fiber alignment. Moreover, methylprednisolone has been shown to exert anti-inflammatory effects without negatively impacting cell activities, suggesting its selective role in modulating inflammation while preserving cell function.[77,78]

As shown in Fig. 12A, multi-layer scaffolds, including EPUD/HG (1 : 10), EPUD/HG (1 : 4), and EPUD/HG (1 : 2), exhibited significant cell attachment. Numerous cells with extensive filopodia were firmly anchored to the hydrogel substrate, showing the scaffolds' biomimetic and favorable environment for cell adhesion. It has been reported that ECM proteins on the substrate can enhance cell attachment.[79] The abundant
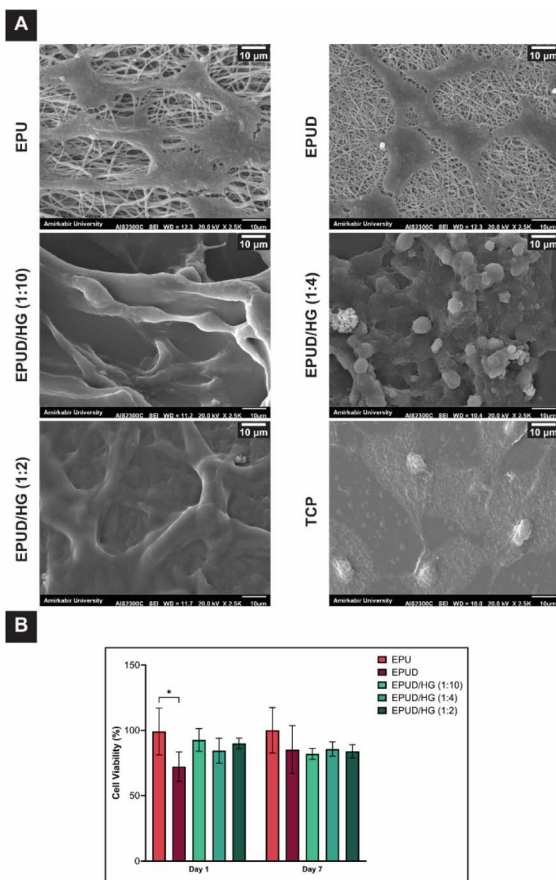
Fig. 12 (A) SEM images of HUVECs on EPU, EPUD, multi-layer scaffolds with different HA : G ratios and TCP; (B) metabolic activity of HUVECs on EPU, EPUD and multi-layer scaffolds after 1 and 7 days of culture. *$p < 0.05$ and $n = 3$.

presence of these proteins in the hydrogel is likely due to the functional groups of gelatin, which contains integrin-binding sites such as RGD motifs that facilitate cell anchoring and adhesion.[80,81] Integrin receptors on cells recognize these specific groups, modulating cellular responses such as adhesion.[79,82] Additionally, hyaluronic acid further contributes to HUVECs behavior. A study by Fiorica *et al.* demonstrated that HA-containing hydrogels support HUVECs activities in both 2D and 3D environments.[83] It has been reported that more hydrophilic substrates cause greater culture medium absorption, which results in increased adsorption of medium proteins and, in turn, enhancements in cell attachment.[55] The results of the swelling test showed that the addition of HA significantly increased the ability of fiber/hydrogel scaffolds to absorb water. Consequently, the incorporation of hyaluronic acid in the hydrogel enhanced endothelial cell behavior, emphasizing HA's role in promoting endothelial activity in hydrogel-based systems.[83,84]

3.9.2. Cell viability. Cell viability is a critical indicator of scaffold performance, reflecting the ability of cells to survive and proliferate within a given environment.[85] Ensuring high cell viability on scaffolds is essential for the successful integration of the material with host tissue in tissue engineering

applications.[17,86] HUVECs were selected for this study due to their relevance in vascular tissue engineering, where they play a pivotal role in angiogenesis and endothelial function.[87]

On day 1, since EPU served as the control for cell viability studies, it showed 100% viability. In contrast, the EPUD exhibited a significant reduction in viability (~70%), which is consistent with previous reports indicating that methylprednisolone can temporarily suppress HUVEC proliferation.[36] Interestingly, the composite scaffolds showed partial recovery of viability on Day 1, with values ranging from about 80% to 90%, depending on the HA : G ratio. Although not all differences were statistically significant, these results suggest that the hydrogel acts as a protective matrix, reducing the acute cytotoxic effects of the drug, as confirmed by drug release studies.

By day 7, EPUD showed modest recovery (~80%), indicating that cells can partially adapt or recover from initial drug-induced stress over time. As shown in the drug release study (Fig. 10), over 85% of the drug was released within 3 days, indicating that the majority of the drug is released by Day 7, allowing cells sufficient time to adapt to the new drug concentration in the culture medium. Composite scaffolds maintained stable viability (~80–82%) during the same period, with no significant differences among the various HA : G ratios. This stability suggests that the hydrogel layers create a microenvironment that supports cell survival, likely by buffering direct drug exposure and providing a more physiologically suitable surface for attachment and proliferation.[88,89] These results highlight the overall biocompatibility of the scaffold components and their suitability for supporting endothelial cells in potential cardiovascular applications.

Although the scaffolds demonstrated excellent early biocompatibility, viability metrics alone do not capture functional behaviors such as angiogenesis or cardiogenesis. Therefore, while the present study focused on establishing the scaffold's architecture, mechanical integrity, and drug-release performance, expanded biological analyses will be pursued in future work.

These multilayer scaffolds are intended for applications such as vascular patches or pre-vascularized cardiac constructs, which are typically implanted *via* surgical procedures. Consistent with other clinically utilized biomaterial grafts, this scaffold would require surgical placement. Future studies will therefore include assessments of suturability, hemodynamic performance, and preclinical implantation to evaluate translational feasibility.

4. Conclusion

In this study, multi-layered scaffolds were successfully developed by integrating methylprednisolone-loaded PU electrospun mats with hydrogels of varying hyaluronic acid-to-gelatin ratios for potential cardiovascular applications. Aligned and bead-free EPU nanofibers were fabricated, and those incorporating methylprednisolone exhibited sustained drug release (>80%) over two weeks in all scaffolds. Incorporating a hydrogel layer (HA : G ratios of 1 : 10, 1 : 4, and 1 : 2) created a three-dimensional scaffold, addressing the limitations of two-

dimensional nanofibrous structures and providing a biomimetic environment conducive to cellular activities. The HA : G ratio significantly influenced scaffold properties. As the HA : G ratio increased (from 1 : 10 to 1 : 2), pore size expanded (∼250 μm to ∼489 μm), swelling capacity increased (∼900% to ∼2246%), and weight loss after 28 days rose (∼83% to ∼93%). Biological assays demonstrated enhanced HUVECs activities. Based on a multi-parameter assessment, the EPUD/HG (1 : 10) scaffold was identified as the optimal composition. This formulation exhibited the highest crosslinking density, mechanical properties closest to native cardiac tissue, a controlled and sustained drug release profile, and degradation behavior compatible with the 4–6 week cardiac repair window, and cell viability within the non-toxic range, supporting its suitability for cardiovascular applications. These findings highlight the potential of drug-releasing multi-layered 3D scaffolds to enhance the bioactivity of tissue-engineered constructs, supporting their application in cardiovascular tissue engineering and other regenerative medicine strategies. Future studies should include extended *in vitro* evaluations using specialized cell types, as well as *in vivo* assessments to examine scaffold integration, vascularization, and functional recovery. Further optimization of scaffold composition and drug delivery strategies may enhance translational potential for cardiovascular tissue regeneration. From a practical perspective, the effects of sterilization, long-term storage, and batch-to-batch reproducibility should also be assessed to facilitate clinical translation.

Author contributions

All authors have contributed significantly to the research and preparation of this manuscript. Reyhaneh Farshbaf Shakib was primarily responsible for conceptualization, methodology, investigation, formal analysis, visualization, and writing – original draft. Dr Masoumeh Haghbin Nazarpak and Dr Atefeh Solouk supervised the project and contributed to supervision, methodology, writing – review & editing, and funding acquisition. Dr Saeid Bahrami contributed to resources, methodology, validation, and writing – review & editing.

Conflicts of interest

The authors have no relevant financial or non-financial interests to disclose.

Data availability

All data generated or analyzed during this study are included in this article.

Acknowledgements

References

1 A. Fakhrali, M. Tamimi, D. Semnani, H. Salehi, A. Ghodsi, S. Rajabi, *et al.*, Electroconductive Nanofiber/Myocardium Gel Scaffolds Applicable for Myocardial Infarction Therapy, *ACS Appl. Polym. Mater.*, 2024, **6**(10), 5593–5607.

2 S. Mehrotra, S. Dey, K. Sachdeva, S. Mohanty and B. Mandal, Recent advances in tailoring stimuli responsive hybrid scaffolds for cardiac tissue engineering and allied applications, *J. Mater. Chem. B*, 2023, **11**(43), 10297–10331.

3 S. Cho, D. E. Discher, K. W. Leong, G. Vunjak-Novakovic and J. C. Wu, Challenges and opportunities for the next generation of cardiovascular tissue engineering, *Nat. Methods*, 2022, **19**(9), 1064–1071.

4 D. Zhao, Epidemiological features of cardiovascular disease in Asia, *Jacc: Asia*, 2021, **1**(1), 1–13.

5 N. Amiryaghoubi, M. Fathi and Y. Javadzadeh, Recent advances in polymer-based scaffolds for cardiac tissue engineering, *Int. J. Polym. Mater. Polym. Biomater.*, 2024, 1–25.

6 M. Shahriari-Khalaji, M. Shafiq, H. Cui, R. Cao and M. Zhu, Advancements in the fabrication technologies and biomaterials for small diameter vascular grafts: A fine-tuning of physicochemical and biological properties, *Appl. Mater. Today*, 2023, **31**, 101778.

7 S. Pilato, S. Moffa, G. Siani, F. Diomede, O. Trubiani, J. Pizzicannella, *et al.*, 3D graphene oxide-polyethylenimine scaffolds for cardiac tissue engineering, *ACS Appl. Mater. Interfaces*, 2023, **15**(11), 14077–14088.

8 S. Eom, S. M. Park, D. G. Hwang, H. W. Kim, J. Jang and D. S. Kim, Fabrication of an align-random distinct, heterogeneous nanofiber mat endowed with bifunctional properties for engineered 3D cardiac anisotropy, *Composites, Part B*, 2021, **226**, 109336.

9 S. Mohammadi Nasr, N. Rabiee, S. Hajebi, S. Ahmadi, Y. Fatahi, M. Hosseini, *et al.*, Biodegradable nanopolymers in cardiac tissue engineering: From concept towards nanomedicine, *Int. J. Nanomed.*, 2020, 4205–4224.

10 Z. Yao, Y. Qian, Y. Jin, S. Wang, J. Li, W.-E. Yuan and C. Fan, Biomimetic multilayer polycaprolactone/sodium alginate hydrogel scaffolds loaded with melatonin facilitate tendon regeneration, *Carbohydr. Polym.*, 2022, **277**, 118865.

11 S. Bahrami, H. Mirzadeh, A. Solouk and D. Duprez, Bioinspired scaffolds based on aligned polyurethane nanofibers mimic tendon and ligament fascicles, *Biotechnol. J.*, 2023, 2300117.

12 C. Rinoldi, E. Kijeńska-Gawrońska, A. Khademhosseini, A. Tamayol and W. Swieszkowski, Fibrous systems as potential solutions for tendon and ligament repair, healing, and regeneration, *Adv. Healthcare Mater.*, 2021, **10**(7), 2001305.

13 F. Tondnevis, H. Keshvari and J. A. Mohandesi, Fabrication, characterization, and *in vitro* evaluation of electrospun polyurethane-gelatin-carbon nanotube scaffolds for cardiovascular tissue engineering applications, *J. Biomed. Mater. Res., Part B*, 2020, **108**(5), 2276–2293.

14 S. Wu, T. Dong, Y. Li, M. Sun, Y. Qi, J. Liu, *et al.*, State-of-the-art review of advanced electrospun nanofiber yarn-based textiles for biomedical applications, *Appl. Mater. Today*, 2022, **27**, 101473.

15 S. Jana, F. Franchi and A. Lerman, Fibrous heart valve leaflet substrate with native-mimicked morphology, *Appl. Mater. Today*, 2021, **24**, 101112.

16 M. Forouharshad, A. Raspa, G. Fortino, M. G. Ciulla, A. Farazdaghi, V. Stolojan, *et al.*, Biomimetic electrospun PVDF/self-assembling peptide piezoelectric scaffolds for neural stem cell transplantation in neural tissue engineering, *RSC Adv.*, 2024, **14**(30), 21277–21291.

17 E. Ghanbari, A. Solouk, R. Mehdinavaz Aghdam, M. Haghbin Nazarpak and S. H. Ahmadi Tafti, A novel substrate based on electrospun polyurethane nanofibers and electrosprayed polyvinyl alcohol microparticles for recombinant human erythropoietin delivery, *J. Biomed. Mater. Res., Part A*, 2022, **110**(1), 181–195.

18 A. A. S. Samson and J. M. Song, Scaffold-free 3D printing for fabrication of biomimetic branched multinucleated cardiac tissue construct: a promising ex vivo model for *in situ* detection of drug-induced sodium ion channel responses, *Appl. Mater. Today*, 2022, **27**, 101416.

19 P. W. Raut, A. A. Shitole, A. Khandwekar and N. Sharma, Engineering biomimetic polyurethane using polyethylene glycol and gelatin for blood-contacting applications, *J. Mater. Sci.*, 2019, **54**(14), 10457–10472.

20 N. Goonoo, Tunable biomaterials for myocardial tissue regeneration: promising new strategies for advanced biointerface control and improved therapeutic outcomes, *Biomater. Sci.*, 2022, **10**(7), 1626–1646.

21 J. M. Unagolla and A. C. Jayasuriya, Hydrogel-based 3D bioprinting: A comprehensive review on cell-laden hydrogels, bioink formulations, and future perspectives, *Appl. Mater. Today*, 2020, **18**, 100479.

22 S. Deepthi, K. Jeevitha, M. N. Sundaram, K. Chennazhi and R. Jayakumar, Chitosan–hyaluronic acid hydrogel coated poly (caprolactone) multiscale bilayer scaffold for ligament regeneration, *Chem. Eng. J.*, 2015, **260**, 478–485.

23 A. N. Abbasi, R. Emadi, A. Valiani, M. Kharaziha and A. Finne-Wistrand, An aligned fibrous and thermosensitive hyaluronic acid-puramatrix interpenetrating polymer network hydrogel with mechanical properties adjusted for neural tissue, *J. Mater. Sci.*, 2022, **57**(4), 2883–2896.

24 A. Serafin, M. Culebras, J. M. Oliveira, J. Koffler and M. N. Collins, 3D printable electroconductive gelatin-hyaluronic acid materials containing polypyrrole nanoparticles for electroactive tissue engineering, *Adv. Compos. Hybrid Mater.*, 2023, **6**(3), 109.

25 L. V. Le, P. Mohindra, Q. Fang, R. E. Sievers, M. A. Mkrtschjan, C. Solis, *et al.*, Injectable hyaluronic acid based microrods provide local micromechanical and biochemical cues to attenuate cardiac fibrosis after myocardial infarction, *Biomaterials*, 2018, **169**, 11–21.

26 D. Gong, Q. Yao, N. Wu, Y. Cai, S. Zhang, H. Chen, *et al.*, 3D microfibrous scaffolds reinforced hyaluronic acid hydrogel for the conjunctival defects repair and ocular surface reconstruction, *Composites, Part B*, 2025, **292**, 112087.

27 Q. Xu, J. E. Torres, M. Hakim, P. M. Babiak, P. Pal, C. M. Battistoni, *et al.*, Collagen-and hyaluronic acid-based hydrogels and their biomedical applications, *Mater. Sci. Eng., R*, 2021, **146**, 100641.

28 J. Li, W. Fang, T. Hao, D. Dong, B. Yang, F. Yao and C. Wang, An anti-oxidative and conductive composite scaffold for cardiac tissue engineering, *Composites, Part B*, 2020, **199**, 108285.

29 S. Bahrami, Design, Fabrication and Evaluation of Polyurethane/Gelatin Fiber/Hydrogel Scaffolds for Tendon Tissue Engineering, PhD thesis, Sorbonne université, 2023.

30 W. L. Lim, L. L. Liau, M. H. Ng, S. R. Chowdhury and J. X. Law, Current progress in tendon and ligament tissue engineering, *Tissue Eng. Regener. Med.*, 2019, **16**, 549–571.

31 A. J. Kuijpers, G. H. Engbers, J. Krijgsveld, S. A. Zaat, J. Dankert and J. Feijen, Cross-linking and characterisation of gelatin matrices for biomedical applications, *J. Biomater. Sci., Polym. Ed.*, 2000, **11**(3), 225–243.

32 J. H. Kim, Y.-J. Choi, H.-G. Yi, J. H. Wang, D.-W. Cho and Y. H. Jeong, A cell-laden hybrid fiber/hydrogel composite for ligament regeneration with improved cell delivery and infiltration, *Biomed. Mater.*, 2017, **12**(5), 055010.

33 Y. Yao, J. Ding, Z. Wang, H. Zhang, J. Xie, Y. Wang, *et al.*, ROS-responsive polyurethane fibrous patches loaded with methylprednisolone (MP) for restoring structures and functions of infarcted myocardium in vivo, *Biomaterials*, 2020, **232**, 119726.

34 P. Yang, Y. Shi, H. Hu, Y. Wang, Y. Wang, X. Li, *et al.*, Inhibition of neuron and cardiac remodeling by microenvironment-responsive injectable hydrogels with sympatho-immune regulation properties for myocardial infarction therapy, *Composites, Part B*, 2025, **297**, 112300.

35 M. Suku, L. Forrester, M. Biggs and M. G. Monaghan, Resident macrophages and their potential in cardiac tissue engineering, *Tissue Eng., Part B*, 2022, **28**(3), 579–591.

36 J.-S. Yoon, H.-H. Kim, J.-W. Han, Y. Lee and J.-S. Lee, Effects of intravenous immunoglobulin and methylprednisolone on human umbilical vein endothelial cells in vitro, *Immunobiology*, 2006, **211**(5), 351–357.

37 L. Ghasemi-Mobarakeh, D. Semnani and M. Morshed, A novel method for porosity measurement of various surface layers of nanofibers mat using image analysis for tissue engineering applications, *J. Appl. Polym. Sci.*, 2007, **106**(4), 2536–2542.

38 S. Bahrami, A. Solouk, D. Duprez and H. Mirzadeh, Microstructure Manipulation of Polyurethane-Based Macromolecular Scaffold for Tendon/Ligament Tissue Engineering, *Macromol. Mater. Eng.*, 2022, **307**(1), 2100584.

39 R. Kale and A. Bajaj, Ultraviolet spectrophotometric method for determination of gelatin crosslinking in the presence of amino groups, *J. Young Pharm.*, 2010, **2**(1), 90–94.

40 M. Delyanee, A. Solouk, S. Akbari and E. Seyedjafari, Modification of electrospun poly (L-lactic acid)/ polyethylenimine nanofibrous scaffolds for biomedical

application, *Int. J. Polym. Mater. Polym. Biomater.*, 2018, **67**(4), 247–257.

41 C. D. Johnson, A. R. D'Amato and R. J. Gilbert, Electrospun fibers for drug delivery after spinal cord injury and the effects of drug incorporation on fiber properties, *Cells Tissues Organs*, 2016, **202**(1–2), 116–135.

42 A. J. Robinson, A. Pérez-Nava, S. C. Ali, J. B. González-Campos, J. L. Holloway and E. M. Cosgriff-Hernandez, Comparative analysis of fiber alignment methods in electrospinning, *Matter*, 2021, **4**(3), 821–844.

43 Y. Cho, J. W. Baek, M. Sagong, S. Ahn, J. S. Nam and I. D. Kim, Electrospinning and nanofiber technology: fundamentals, innovations, and applications, *Adv. Mater.*, 2025, **37**(28), 2500162.

44 T. A. Karimi, S. Karbasi, E. Naghashzargar and H. Salehi, Biodegradation and cellular evaluation of aligned and random poly (3-hydroxybutyrate)/chitosan electrospun scaffold for nerve tissue engineering applications, *Mater. Technol.*, 2020, **35**(2), 92–101.

45 F. Zhang, C. He, L. Cao, W. Feng, H. Wang, X. Mo and J. Wang, Fabrication of gelatin–hyaluronic acid hybrid scaffolds with tunable porous structures for soft tissue engineering, *Int. J. Biol. Macromol.*, 2011, **48**(3), 474–481.

46 B. Khabbaz, A. Solouk and H. Mirzadeh, Polyvinyl alcohol/soy protein isolate nanofibrous patch for wound-healing applications, *Prog. Biomater.*, 2019, **8**, 185–196.

47 J. Xing, N. Liu, N. Xu, W. Chen and D. Xing, Engineering complex anisotropic scaffolds beyond simply uniaxial alignment for tissue engineering, *Adv. Funct. Mater.*, 2022, **32**(15), 2110676.

48 A. Serafin, M. Culebras and M. N. Collins, Synthesis and evaluation of alginate, gelatin, and hyaluronic acid hybrid hydrogels for tissue engineering applications, *Int. J. Biol. Macromol.*, 2023, **233**, 123438.

49 J. Amirian, T. Sultana, G. J. Joo, C. Park and B.-T. Lee, In vitro endothelial differentiation evaluation on polycaprolactone-methoxy polyethylene glycol electrospun membrane and fabrication of multilayered small-diameter hybrid vascular graft, *J. Biomater. Appl.*, 2020, **34**(10), 1395–1408.

50 S. Bahrami, A. Solouk, H. Mirzadeh and A. M. Seifalian, Electroconductive polyurethane/graphene nanocomposite for biomedical applications, *Composites, Part B*, 2019, **168**, 421–431.

51 X. Zhao, Y. H. Qi, K. J. Li and Z. P. Zhang, Hydrogen bonds and FTIR peaks of polyether polyurethane-urea, *Key Eng. Mater.*, 2019, **815**, 151–156.

52 M. Keikha, E. Entekhabi, M. Shokrollahi, M. H. Nazarpak, Z. Hassannejad, S. Akbari, *et al.*, Fabrication and characterization of methylprednisolone-loaded polylactic acid/hyaluronic acid nanofibrous scaffold for soft tissue engineering, *J. Ind. Text.*, 2022, **52**, 15280837221116593.

53 M. V. Natu, J. P. Sardinha, I. J. Correia and M. Gil, Controlled release gelatin hydrogels and lyophilisates with potential application as ocular inserts, *Biomed. Mater.*, 2007, **2**(4), 241.

54 N. Ashok, D. Sankar and R. Jayakumar, Surface Modified Polymeric Nanofibers in Tissue Engineering and Regenerative Medicine, *Electrospun Polymeric Nanofibers:*

Insight into Fabrication Techniques and Biomedical Applications, Springer, 2023, pp. 177–189.

55 Z. Z. Eivazi, A. Solouk, M. Shafieian and M. H. Nazarpak, Electrospun polyurethane/carbon nanotube composites with different amounts of carbon nanotubes and almost the same fiber diameter for biomedical applications, *Mater. Sci. Eng. C*, 2021, **118**, 111403.

56 C. Rinoldi, M. Costantini, E. Kijeńska-Gawrońska, S. Testa, E. Fornetti, M. Heljak, *et al.*, Tendon tissue engineering: effects of mechanical and biochemical stimulation on stem cell alignment on cell-laden hydrogel yarns, *Adv. Healthcare Mater.*, 2019, **8**(7), 1801218.

57 W. Kong, Y. Gao, Q. Liu, L. Dong, L. Guo, H. Fan, *et al.*, The effects of chemical crosslinking manners on the physical properties and biocompatibility of collagen type I/hyaluronic acid composite hydrogels, *Int. J. Biol. Macromol.*, 2020, **160**, 1201–1211.

58 S.-H. Chen, C.-H. Chen, K. Shalumon and J.-P. Chen, Preparation and characterization of antiadhesion barrier film from hyaluronic acid-grafted electrospun poly (caprolactone) nanofibrous membranes for prevention of flexor tendon postoperative peritendinous adhesion, *Int. J. Nanomed.*, 2014, 4079–4092.

59 G. Yang, B. B. Rothrauff and R. S. Tuan, Tendon and ligament regeneration and repair: clinical relevance and developmental paradigm, *Birth Defects Res., Part C*, 2013, **99**(3), 203–222.

60 Y. Liu, L. Ren and Y. Wang, Crosslinked collagen–gelatin–hyaluronic acid biomimetic film for cornea tissue engineering applications, *Mater. Sci. Eng. C*, 2013, **33**(1), 196–201.

61 K.-C. Chang, W.-C. Chen, C.-H. Chen, C.-L. Ko, S.-M. Liu and J.-C. Chen, Chemical cross-linking on gelatin-hyaluronan loaded with hinokitiol for the preparation of guided tissue regeneration hydrogel membranes with antibacterial and biocompatible properties, *Mater. Sci. Eng. C*, 2021, **119**, 111576.

62 Y. S. Choi, S. R. Hong, Y. M. Lee, K. W. Song, M. H. Park and Y. S. Nam, Studies on gelatin-containing artificial skin: II. Preparation and characterization of cross-linked gelatin-hyaluronate sponge, *J. Biomed. Mater. Res.*, 1999, **48**(5), 631–639.

63 K. Jarquín-Yáñez, J. Arenas-Alatorre, G. Piñón-Zárate, R. Arellano-Olivares, M. Herrera-Enríquez, B. Hernández-Téllez and A. Castell-Rodríguez, Structural effect of different EDC crosslinker concentration in gelatin-hyaluronic acid scaffolds, *J Bioeng Biomed Sci.*, 2016, **6**, 182.

64 L. Meng, J. He and C. Pan, Research progress on hydrogel–elastomer adhesion, *Materials*, 2022, **15**(7), 2548.

65 J. Ma, J. Li, S. Hu, X. Wang, M. Li, J. Xie, *et al.*, Collagen modified anisotropic PLA scaffold as a base for peripheral nerve regeneration, *Macromol. Biosci.*, 2022, **22**(7), 2200119.

66 Y. Qu, J. Tang, L. Liu, L. Song, S. Chen and Y. Gao, α-Tocopherol liposome loaded chitosan hydrogel to suppress oxidative stress injury in cardiomyocytes, *Int. J. Biol. Macromol.*, 2019, **125**, 1192–1202.

© 2026 The Author(s). Published by the Royal Society of Chemistry

67 E. Chiani, A. Beaucamp, Y. Hamzeh, M. Azadfallah, A. Thanusha and M. N. Collins, Synthesis and characterization of gelatin/lignin hydrogels as quick release drug carriers for Ribavirin, *Int. J. Biol. Macromol.*, 2023, **224**, 1196–1205.

68 F. Moztarzadeh, M. Farokhi, A. A. Mehrizi, H. Basiri and S. S. Mohseni, Preparation of microfluidic-based pectin microparticles loaded carbon dots conjugated with BMP-2 embedded in gelatin-elastin-hyaluronic acid hydrogel scaffold for bone tissue engineering application, *Int. J. Biol. Macromol.*, 2021, **184**, 29–41.

69 A. Thanusha, S. Mohanty, A. K. Dinda and V. Koul, Fabrication and evaluation of gelatin/hyaluronic acid/ chondroitin sulfate/asiatic acid based biopolymeric scaffold for the treatment of second-degree burn wounds– Wistar rat model study, *Biomed. Mater.*, 2020, **15**(5), 055016.

70 E. Csapó, H. Szokolai, Á. Juhász, N. Varga, L. Janovák and I. Dékány, Cross-linked and hydrophobized hyaluronic acid-based controlled drug release systems, *Carbohydr. Polym.*, 2018, **195**, 99–106.

71 R. W. Korsmeyer, R. Gurny, E. Doelker, P. Buri and N. A. Peppas, Mechanisms of solute release from porous hydrophilic polymers, *Int. J. Pharm.*, 1983, **15**(1), 25–35.

72 J. A. Roacho-Pérez, E. N. Garza-Treviño, N. K. Moncada-Saucedo, P. A. Carriquiry-Chequer, L. E. Valencia-Gómez, E. R. Matthews, *et al.*, Artificial scaffolds in cardiac tissue engineering, *Life*, 2022, **12**(8), 1117.

73 J. E. Pomeroy, A. Helfer and N. Bursac, Biomaterializing the promise of cardiac tissue engineering, *Biotechnol. Adv.*, 2020, **42**, 107353.

74 P. Ahmadi, N. Nazeri, M. A. Derakhshan and H. Ghanbari, Preparation and characterization of polyurethane/chitosan/ CNT nanofibrous scaffold for cardiac tissue engineering, *Int. J. Biol. Macromol.*, 2021, **180**, 590–598.

75 K. Roshanbinfar, L. Vogt, F. Ruther, J. A. Roether, A. R. Boccaccini and F. B. Engel, Nanofibrous composite with tailorable electrical and mechanical properties for cardiac tissue engineering, *Adv. Funct. Mater.*, 2020, **30**(7), 1908612.

76 F. Koeini, A. Solouk and S. Akbari, Graphene Oxide-Incorporated Polylactic Acid/Polyamidoamine Dendrimer Electroconductive Nanocomposite as a Promising Scaffold for Guided Tissue Regeneration, *Macromol. Mater. Eng.*, 2024, 2400100.

77 J. Liu, H. Zhu, Y. Pei, H. Zhang, J. Zhou and Z. Jing, A methylprednisolone-loaded and core-shell nanofiber-covered stent-graft to prevent inflammation and reduce degradation in aortic dissection, *Biomater. Res.*, 2022, **26**(1), 15.

78 G. Mullins, J. Sunden-Cullberg, A. S. Johansson, A. Rouhiainen, H. Erlandsson-Harris, H. Yang, *et al.*, Activation of human umbilical vein endothelial cells leads to relocation and release of high-mobility group box

chromosomal protein 1, *Scand. J. Immunol.*, 2004, **60**(6), 566–573.

79 J. Zhang, X. Ma, D. Lin, H. Shi, Y. Yuan, W. Tang, *et al.*, Magnesium modification of a calcium phosphate cement alters bone marrow stromal cell behavior *via* an integrin-mediated mechanism, *Biomaterials*, 2015, **53**, 251–264.

80 M. Chen, Y. Zhang, W. Zhang and J. Li, Polyhedral oligomeric silsesquioxane-incorporated gelatin hydrogel promotes angiogenesis during vascularized bone regeneration, *ACS Appl. Mater. Interfaces*, 2020, **12**(20), 22410–22425.

81 D. Gupta, J. Venugopal, M. P. Prabhakaran, V. G. Dev, S. Low, A. T. Choon and S. Ramakrishna, Aligned and random nanofibrous substrate for the *in vitro* culture of Schwann cells for neural tissue engineering, *Acta Biomater.*, 2009, **5**(7), 2560–2569.

82 S. M. Saraiva, S. P. Miguel, M. P. Ribeiro, P. Coutinho and I. J. Correia, Synthesis and characterization of a photocrosslinkable chitosan–gelatin hydrogel aimed for tissue regeneration, *RSC Adv.*, 2015, **5**(78), 63478–63488.

83 C. Fiorica, F. S. Palumbo, G. Pitarresi, M. Allegra, R. Puleio and G. Giammona, Hyaluronic acid and α-elastin based hydrogel for three dimensional culture of vascular endothelial cells, *J. Drug Delivery Sci. Technol.*, 2018, **46**, 28–33.

84 K. Sugibayashi, Y. Kumashiro, T. Shimizu, J. Kobayashi and T. Okano, A molded hyaluronic acid gel as a micro-template for blood capillaries, *J. Biomater. Sci., Polym. Ed.*, 2013, **24**(2), 135–147.

85 N. Amiryaghoubi, M. Fathi and Y. Javadzadeh, Recent advances in polymer-based scaffolds for cardiac tissue engineering, *Int. J. Polym. Mater. Polym. Biomater.*, 2024, **73**(17), 1500–1524.

86 P. Davoudi, S. Assadpour, M. A. Derakhshan, J. Ai, A. Solouk and H. Ghanbari, Biomimetic modification of polyurethane-based nanofibrous vascular grafts: A promising approach towards stable endothelial lining, *Mater. Sci. Eng. C*, 2017, **80**, 213–221.

87 D. J. Medina-Leyte, M. Domínguez-Pérez, I. Mercado, M. T. Villarreal-Molina and L. Jacobo-Albavera, Use of human umbilical vein endothelial cells (HUVEC) as a model to study cardiovascular disease: A review, *Appl. Sci.*, 2020, **10**(3), 938.

88 A. J. Campillo-Fernández, R. E. Unger, K. Peters, S. Halstenberg, M. Santos, M. S. Sánchez, *et al.*, Analysis of the biological response of endothelial and fibroblast cells cultured on synthetic scaffolds with various hydrophilic/ hydrophobic ratios: influence of fibronectin adsorption and conformation, *Tissue Eng., Part A*, 2009, **15**(6), 1331–1341.

89 A. Aljawish, L. Muniglia, J. Jasniewski, A. Klouj, J. Scher and I. Chevalot, Adhesion and growth of HUVEC endothelial cells on films of enzymatically functionalized chitosan with phenolic compounds, *Process Biochem.*, 2014, **49**(5), 863–871.